Journal of Energy and Power Engineering 7 (2013) 1669-1680

Numerical Study of Forced Convection Lid-Driven Cavity Flows Using LES (Large Eddy Simulation)

Elizaldo D. dos Santos[1], Adriane P. Petry[2], Luiz A.O. Rocha[2] and Francis H.R. França[2]

1. Escola de Engenharia, Universidade Federal do Rio Grande, Porto Alegre 96201-090, RS, Brasil

2. Departamento de Engenharia Mecânica, Universidade Federal do Rio Grande do Sul, Porto Alegre 90050-170, RS, Brasil

Received: May 18, 2012 / Accepted: August 21, 2012 / Published: September 30, 2013.

Abstract: This study presents the LES (large eddy simulation) of forced convection in laminar and two dimensional turbulent flows when the flow reaches the steady state. The main purpose is the evaluation of a developed numerical methodology for the simulation of forced convection flows at various Reynolds numbers ($100 \leq Re_H \leq 10{,}000$) and for a fixed Prandtl number ($Pr = 1.0$). The hexahedral eight-node FEM (finite element method) with an explicit Taylor-Galerkin scheme is used to obtain the numerical solutions of the conservation equations of mass, momentum and energy. The Smagorinsky model is employed for the sub-grid treatment. The time-averaged velocity and temperature profiles are compared with results of literature and a CFD (computational fluid dynamics) package based on finite volume method, leading to a highest deviation of nearly 6%. Moreover, characteristics of the forced convection flows are properly obtained, e.g., the effect of the Reynolds number over the multiplicity of scales.

Key words: LES, FEM, forced convection, driven cavity, energy equation.

1. Introduction

The convection heat transfer is very important in many of engineering applications (heat exchangers, turbines, compressors, cooling of electronic packages) as well as in natural phenomena (pollutants dispersion in atmospheric layer, steam transport by rivers and oceans evaporation). Moreover, many of these flows are turbulent, especially in practical applications. However, there are several difficulties for the comprehension and evaluation of these kinds of flows. In this sense, researches rely on experimental and numerical techniques [1, 2].

Concerning the numerical approach of turbulent flows, different methods can be attempted. The DNS (direct numerical simulation) is the most accurate, depending solely on the numerical schemes, and leading to results that are comparable to those obtained in experiments [3]. However, DNS requires a large computational effort to solve all the involved scales. For isothermal flows, the set of equations to be simultaneously solved is in the order of $Re^{9/4}$. For convection heat transfer flows, this set of equations is increased as function of the Prandtl number (Pr). According to Pope et al. [2, 4], the grid points are required in the order of $Pr^3Re^{9/4}$ and $Pr^{3/2}Re^{9/4}$, respectively. This fact limits its application to simple geometries with low Reynolds numbers. On the other hand, the classical RANS (Reynolds-averaged Navier-Stokes) model requires less computational effort, but the turbulence models are far from universal and can not correctly predict some unsteady phenomena, such as shedding of Karman vortices in a wake or Kelvin-Helmholtz vortices in a mixing layer [5]. The other approach is the LES (large eddy simulation), which is based on eliminating smaller scales than a cutoff length with the use of a spatial filter and directly solving the larger scales [3, 6]. This approach allows the estimation of the instantaneous

Corresponding author: Elizaldo D. dos Santos, mechanical engineering, DSc., research fields: turbulence, computational fluid dynamics, heat transfer, geometrical optimization and constructal design. E-mail: elizaldosantos@furg.br.

fields for Reynolds numbers larger than those treated with the DNS, and with a more universal behavior than RANS. However, LES requires grids more refined than those employed for RANS simulations, and depends on closure models for the estimation of the behavior of the small scales. Saugat [6] classified the closure models into functional modeling, which is based on representing kinetic energy transfer (Smagorinsky, structure function and dynamical models) and structural modeling, which aims at reproducing the eigenvectors of the statistical correlation tensors of the sub-grid modes.

Concerning the evaluation of developed models for the simulation of convection turbulent flows, the simulation of lid-driven cavity flows is, in general, attractive due to its simple geometry and well posed boundary conditions, together with the presence of complex phenomena such as the boundary detachment and reattachment, generation of primary and secondary vortices [7, 8]. Moreover, experimental studies in cavities have been carried out aiming at generating data for model validations [7]. In this sense, simulations of forced convection lid-driven cavity flows are performed in the present work.

For lid-driven cavity isothermal flows, it is important to mention the important work of Ref. [7], which performed a number of experiments for flows considering laminar and turbulent regimes, generating results for the average velocity fields and statistics of turbulence. These results served as benchmark solution for several other numerical studies [9, 10]. Into the numerical scope, several methods have been developed for the simulation of isothermal turbulent cavity flows, e.g., Erturk and Gökçöl [11] developed a forth-order formulation of steady 2D incompressible Navier-Stokes for flows at Reynolds numbers (Re_H) ranging from 10,000 to 20,000, Guia et al. [12] simulated laminar and turbulent flows at two-dimensional domains for Reynolds numbers of Re_H = 1,000 and 10,000 using a model named multi-grid. Petry and Awruch [13] validated the isothermal version of the code employed in the present work for 3D lid-driven cavity flows at Reynolds numbers of 3,200 and 10,000. In the latter work, the mean velocity profiles and the statistics of turbulence were compared with the experimental results of Ref. [7].

For the heat transfer problems in cavities with turbulent incompressible flows, the efforts have been focused on natural convection considering RANS [14], LES [15] and DNS [16]. In the mixed convection heat transfer, it is possible to mention the works [17, 18] into the RANS framework and Ref. [8] into the LES framework. In the latter work, the same method used here was employed to evaluate the influence of the kind of stratification (stable/unstable) on the fluid dynamics and thermal behavior of turbulent flows. Moreover, the method was validated for the simulation of laminar and turbulent flows. However, this numerical method was not evaluated for the simulation of forced convection flows.

In the present work, the main goal is to investigate the use of the present methodology for the prediction of forced convection, two-dimensional, laminar and turbulent flows at the steady state with the use of the LES approach as a function of several Reynolds numbers. In spite of the fact that turbulence is a three-dimensional phenomenon, in the present case, even at high-Reynolds numbers, the driven-cavity flows display only subtle 3D effects. Then, the simplification of two-dimensional flow is employed here. The same simplification for the LES approach has been presented in Refs. [8, 19, 20].

The simulations of the present method employ the FEM (finite element method), with eight-node isoparametric hexahedral finite element, to solve the mass, momentum and energy equations [21, 22]. The spatial discretization follows the Galerkin method, and the time advance follows an iterative explicit scheme whose expansion of second order is performed with the Taylor series [23]. To avoid some of the convergence difficulties of incompressible flows, the quasi-incompressibility method is used [24]. The

turbulence is tackled with the LES approach using the classical sub-grid Smagorinsky model [25]. To evaluate the behavior of the present method for forced convection flows at the steady state, simulations are performed for various Reynolds numbers of $Re_H = 100$, 1,000 and 10,000 and a fixed Prandtl number of $Pr = 1$. The results for time-averaged velocity and temperature profiles at the center cavity obtained with the present method are compared with those ones presented in Refs. [12, 26, 27]. Moreover, all results are also compared with a CFD (computational fluid dynamics) package based on the finite volume method (FLUENT®) [28].

2. Mathematical Modeling

The modeling of quasi-incompressible, transient and non-isothermal flows is based on the solution of the conservation equations together with the boundary and the initial conditions. In the LES approach, the mass, momentum and energy equations are spatially filtered with a box filter [29]. These equations can be written in an orthonormal basis as:

$$\frac{\partial \overline{P}}{\partial t} + C^2 \frac{\partial}{\partial x_j}\left(\overline{\rho v_j}\right) = 0 \quad (j = 1, 2 \text{ and } 3) \text{ in } t \times \Omega \quad (1)$$

$$\frac{\partial}{\partial t}\left(\overline{\rho v_i}\right) + \frac{\partial}{\partial x_j}\left(\overline{\rho v_i v_j}\right) + \frac{\partial \overline{P}}{\partial x_j}\delta_{ij} - \frac{\partial}{\partial x_j}\left\{\overline{\rho \upsilon}\left(\frac{\partial \overline{v_i}}{\partial x_j} + \frac{\partial \overline{v_j}}{\partial x_i}\right) + \lambda \frac{\partial \overline{v_k}}{\partial x_k}\delta_{ij}\right\} + \frac{\partial\left(\overline{\rho \tau_{ij}}\right)}{\partial x_j} + \overline{\rho} g_i \beta(\overline{T} - T_0) = 0$$

$$(i, j, k = 1, 2 \text{ and } 3) \text{ in } t \times \Omega \quad (2)$$

$$\frac{\partial \overline{T}}{\partial t} + \frac{\partial}{\partial x_j}\left(\overline{v_j T}\right) - \frac{\partial}{\partial x_j}\left\{\alpha \frac{\partial \overline{T}}{\partial x_j} - q_j\right\} - \overline{q'''} = 0$$

$$(j = 1, 2 \text{ and } 3) \text{ in } t \times \Omega \quad (3)$$

where, $\overline{(\,)}$ represent the large scales; ρ is the density of the fluid (kg/m^3); β is the thermal expansion coefficient (K^{-1}); C is the sound propagation speed (m/s); μ is the dynamic viscosity (kg/ms); λ is the volumetric viscosity (kg/ms); υ is the kinematic viscosity (m^2/s); α is the thermal diffusivity (m^2/s); v_i is the velocity in i-direction, i = 1, 2 and 3 (m/s); x_i corresponds to the spatial coordinate, i = 1, 2 and 3 (m); P is the pressure (N/m²); T is the temperature (K); T_0 is a reference temperature (K); g_i is the gravity acceleration in i-direction, i = 1, 2 and 3 (m/s^2); δ_{ij} is the Kronecker delta; Ω is the spatial domain (m); t represents the time domain (s); q''' is the heat source term (W/m^3). The terms τ_{ij} and q_j that arise in the filtering process of the momentum and energy conservation equation, respectively, need to be modeled and can be written by:

$$\tau_{ij} = \overline{v_i v_j} - \overline{v}_i \overline{v}_j \quad (i, j = 1, 2 \text{ and } 3) \quad (4)$$

$$q_j = \overline{v_j T} - \overline{v}_j \overline{T} \quad (j = 1, 2 \text{ and } 3) \quad (5)$$

The first term of the right-hand side of Eqs. (4) and (5) presents the filtered product of instantaneous fields (velocity-velocity and velocity-temperature).

2.1 Smagorinsky Sub-grid Model (SSGS)

The SSGS (Smagorinsky sub-grid scale) model [25] is based on the hypothesis of Boussinesq's eddy viscosity, and takes into consideration the local equilibrium between the production and the dissipation of the sub-grid turbulent stresses. For quasi-incompressible flows, the turbulent tensor can be written as:

$$\tau_{ij} = \upsilon_{sgs}\left(\frac{\partial \overline{v_i}}{\partial x_j} + \frac{\partial \overline{v_j}}{\partial x_i}\right) (i, j = 1,2 \text{ and } 3) \quad (6)$$

where, υ_{sgs} is the kinematic eddy viscosity (m^2/s). The turbulent transport of the thermal energy is obtained by an analogy with the sub-grid Reynolds tensor [10], and is given by:

$$q_j = \alpha_{sgs} \frac{\partial \overline{T}}{\partial x_j} \quad (j = 1, 2 \text{ and } 3) \quad (7)$$

where, α_{sgs} is the thermal eddy diffusivity (m^2/s).

According to the model, the kinematic eddy viscosity is given by:

$$\upsilon_{sgs} = C_S^2 \overline{\Delta}^2 \left|\overline{S}\right| \quad (8)$$

where, C_s is the Smagorinsky constant; $\overline{\Delta}$ is a sub-grid scale characteristic length; $\left|\overline{S}\right|$ is the strain-rate of the filtered field; and $\overline{S}_{ij}$ is the deformation rate of the velocity fields (in s^{-1}). The three last terms are given by:

$$\overline{\Delta} = \sqrt[3]{\prod_{i=1}^{3} \Delta x_i} \quad (i = 1, 2 \text{ and } 3) \quad (9)$$

$$\left|\overline{S}\right| = \sqrt{2 \overline{S}_{ij} \overline{S}_{ij}} \quad (i, j = 1, 2 \text{ and } 3) \quad (10)$$

$$\overline{S}_{ij} = \frac{1}{2}\left(\frac{\partial \overline{v}_i}{\partial x_j} + \frac{\partial \overline{v}_j}{\partial x_i}\right) (i, j = 1, 2 \text{ and } 3) \quad (11)$$

The thermal eddy diffusivity is obtained from a relation between the kinematic eddy viscosity (υ_{sgs}) and

the turbulent Prandtl number (Pr_{sgs}), as given by:

$$\alpha_{sgs} = \frac{C_S^2}{\mathrm{Pr}_{sgs}} \bar{\Delta}^2 \left|\bar{S}\right| \tag{12}$$

The Smagorinsky constant and the turbulent Prandtl number are prescribed here $C_S = 0.23$ and $Pr_{sgs} = 0.6$.

3. Numerical Modeling

3.1 Present Method (Explicit Iterative of Taylor-Galerkin Scheme)

The FEM is employed to obtain the numerical solutions of the equations of that model, the two-dimensional heat transfer in quasi-incompressible, laminar and turbulent flows [21, 22, 29]. The Galerkin method with linear eight-node hexahedral element, also known as Bubnov-Galerkin, is employed for the spatial discretization. The iterative, explicit Taylor-Galerkin scheme of second-order is adopted for the temporal discretization [23]. The temporal scheme is also employed for the stabilization of the numerical solution, since the Galerkin method leads to oscillations in advective-dominated flows [29]. The main steps for the solution of the conservation equations from the FEM are extensively presented on the Ref. [22] and for brevity will not be described here. The variations of pressures, velocities and temperature at each time and iteration step are presented in its matrix forms, as given by:

$$\mathbf{M}_{DP}\Delta\bar{\underset{\sim}{P}}_{k+1}^{n+1} = -\Delta t\left\{\left[\mathbf{G}_j^T\left(\bar{\underset{\sim}{v}}_j\right)^n\right] + \frac{1}{2}\left[\mathbf{G}_j^T\left(\Delta\bar{\underset{\sim}{v}}_j\right)_k^{n+1}\right]\right\} - \left(\mathbf{M}_P - \mathbf{M}_{DP}\right)\Delta\bar{\underset{\sim}{P}}_k^{n+1} \tag{13}$$

$$\mathbf{M}_{DV}\Delta\left(\bar{\underset{\sim}{v}}\right)_{k+1}^{n+1} = -\Delta t\left\{\left[\mathbf{A}_j\left(\bar{\underset{\sim}{v}}\right) + \mathbf{D}_{ij}\left(\bar{\underset{\sim}{v}}_j\right) - \mathbf{G}_i\bar{\underset{\sim}{P}}\right]^n - \frac{1}{2}\left(\left(\mathbf{F}_i - \mathbf{B}_i\bar{\underset{\sim}{T}}\right)^n + \left(\Delta\mathbf{F}_i - \mathbf{B}_i\Delta\bar{\underset{\sim}{T}}\right)_k^{n+1}\right)\right\} \tag{14}$$

$$-\frac{\Delta t}{2}\left\{\mathbf{A}_j\left(\Delta\bar{\underset{\sim}{v}}\right) + \mathbf{D}_{ij}\left(\Delta\bar{\underset{\sim}{v}}_j\right) - \mathbf{G}_i\Delta\bar{\underset{\sim}{P}} + \frac{2}{\Delta t}\left(\mathbf{M}_V - \mathbf{M}_{DV}\right)\Delta\bar{\underset{\sim}{v}}_j\right\}_k^{n+1}$$

$$\mathbf{M}_{DT}\Delta\left(\bar{\underset{\sim}{T}}\right)_{k+1}^{n+1} = -\Delta t\left\{\left[\mathbf{A}_{jT}\left(\bar{\underset{\sim}{T}}\right) + \mathbf{D}_{jT}\left(\bar{\underset{\sim}{T}}\right)\right]^n - \frac{1}{2}\left(\mathbf{F}_T^n + \left(\Delta\mathbf{F}_T\right)_k^{n+1}\right)\right\} \tag{15}$$

$$-\frac{\Delta t}{2}\left\{\mathbf{A}_j\left(\Delta\bar{\underset{\sim}{T}}\right) + \mathbf{D}_{ij}\left(\Delta\bar{\underset{\sim}{T}}\right) + \frac{2}{\Delta t}\left(\mathbf{M}_T - \mathbf{M}_{DT}\right)\Delta\bar{\underset{\sim}{T}}\right\}_k^{n+1}$$

where, $\mathbf{M}_{DP}$, $\mathbf{M}_{DV}$ and $\mathbf{M}_{DT}$ are the discrete matrices for pressure, velocity and temperature, respectively; $\mathbf{M}_P$, $\mathbf{M}_V$ and $\mathbf{M}_T$ are the consistent matrices for pressure, velocity and temperature, respectively; $\mathbf{A}_j$ and $\mathbf{A}_{jT}$ are the advective matrices for momentum and energy; $\mathbf{D}_{ij}$ and $\mathbf{D}_{jT}$ are the diffusion matrices for momentum and energy; $\mathbf{G}_{jT}$ is the matrix that carries the velocity divergent terms; $\mathbf{G}_i$ is the matrix of pressure gradients; the matrix $\mathbf{F}_i$ contains the buoyancy force terms as a function of the reference temperature and the Neumann boundary conditions (surface forces); the matrix $\mathbf{B}_i$ carries the force terms that are dependent of the temperature field; and finally, the matrix $\mathbf{F}_T$ contains the terms of volumetric heat generation and the Neumann boundary conditions (prescribed fluxes). The superscripts (n) and ($n + 1$) are related to the time steps in t and $t + \Delta t$, the subscript k indicates the iterative step and the subscript ~ represents nodal values of the primary variables. The matrices that are shown in Eqs. (13)-(15) are given by:

$$\mathbf{M}_p = \int_{\Omega^e} \underset{\sim}{\psi}^T \underset{\sim}{\psi}\, d\Omega^e \;\text{-}\; \mathbf{M}_v = \int_{\Omega^e} \rho_0 \underset{\sim}{\phi}^T \underset{\sim}{\phi}\, d\Omega^e \;\text{-}\; \mathbf{M}_T = \int_{\Omega^e} \underset{\sim}{\theta}^T \underset{\sim}{\theta}\, d\Omega^e \tag{16}$$

$$\mathbf{A}_j = \int_{\Omega^e} \rho_0 \left(\underset{\sim}{\phi}^T \underset{\sim}{\phi}\right)\bar{\underset{\sim}{v}}_j \frac{\partial \underset{\sim}{\phi}^T}{\partial x_j} d\Omega^e \;\text{-}\; \mathbf{A}_{jT} = \int_{\Omega^e} \left(\underset{\sim}{\theta}^T \underset{\sim}{\phi}\right)\bar{\underset{\sim}{v}}_j \frac{\partial \underset{\sim}{\theta}^T}{\partial x_j} d\Omega^e \tag{17}$$

$$\mathbf{D}_{ij} = \begin{cases} \rightarrow i = 1, k = 2,3; \rightarrow i = 2, k = 3,1; \rightarrow i = 3, k = 1,2 \\ \displaystyle\int_{\Omega^e} \rho_0 \left[2\left(\upsilon + \upsilon_t\right) + \frac{\lambda}{\rho_0}\right]\left(\frac{\partial \underset{\sim}{\phi}^T}{\partial x_i}\frac{\partial \underset{\sim}{\phi}}{\partial x_i}\right) d\Omega^e + \int_{\Omega^e} \rho_0 \left(\upsilon + \upsilon_t\right)\left(\frac{\partial \underset{\sim}{\phi}^T}{\partial x_k}\frac{\partial \underset{\sim}{\phi}}{\partial x_k}\right) d\Omega^e \\ \rightarrow i \neq j \\ \displaystyle\int_{\Omega^e} \rho_0 \left(\upsilon + \upsilon_t\right)\left(\frac{\partial \underset{\sim}{\phi}^T}{\partial x_i}\frac{\partial \underset{\sim}{\phi}}{\partial x_j}\right) d\Omega^e + \int_{\Omega^e} \lambda\left(\frac{\partial \underset{\sim}{\phi}^T}{\partial x_j}\frac{\partial \underset{\sim}{\phi}}{\partial x_i}\right) d\Omega^e \end{cases} \tag{18}$$

$$\mathbf{D}_{jT} = \int_{\Omega^e} \left(\alpha + \alpha_t\right)\frac{\partial \underset{\sim}{\theta}^T}{\partial x_j}\frac{\partial \underset{\sim}{\theta}}{\partial x_j} d\Omega^e$$

$$\mathbf{G}_i = \int_{\Omega^e} \frac{\partial \underset{\sim}{\phi}^T}{\partial x_i} \underset{\sim}{\psi}\, d\Omega^e \;\text{-}\; \mathbf{G}_j^T = \int_{\Omega} \rho_0 C^2 \underset{\sim}{\psi}^T \frac{\partial \underset{\sim}{\phi}}{\partial x_j} d\Omega^e \tag{19}$$

$$\begin{aligned} \mathbf{B}_i &= \int_{\Omega^e} \rho_0 g_i \beta \left(\underset{\sim}{\phi}^T \underset{\sim}{\theta}\right) d\Omega^e \\ \mathbf{F}_i &= \int_{\Omega^e} \underset{\sim}{\phi}\, \rho_0 g_i \beta T_0 d\Omega^e + \int_{\Gamma^e} \underset{\sim}{\phi}\, S_i d\Gamma^e \\ \mathbf{F}_\mathbf{T} &= \int_{\Omega^e} \underset{\sim}{\theta}\, q''' d\Omega^e + \int_{\Gamma^e} \underset{\sim}{\theta}\, \hat{q} d\Gamma^e \end{aligned} \tag{20}$$

where, ψ, ϕ and θ are the vectors of interpolation functions for the pressure (constant), velocity (linear) and temperature (linear), respectively. The superscripts T and e stand for transposed matrix and the element domain.

Since the temporal scheme is explicit, it is necessary to satisfy the Courant's stability condition [24]. Accordingly, the critical time step is given by:

$$\Delta t \leq \frac{\Delta x_i(\min)}{(C + V)} \tag{21}$$

where, Δx_i (min) is the smallest element in the domain (m), V is a reference velocity (m/s), which in this study is taken as the velocity of the sliding plate and C is the sound propagation speed (m/s).

3.2 Numerical Procedures Used in the FLUENT Simulations

All studied cases were also simulated using the CFD package based on hexahedral finite volume method (FLUENT®) [28]. The solver is pressure based and all simulations were performed with second-order bounded central differencing scheme and implicit temporal discretizations. The bounded central differencing scheme employed in the LES simulations consists of a mixture of two advection schemes: central differencing for regions where the flow is diffusive and upwind of second order for regions where advection is dominant [30-32]. The velocity-pressure coupling is performed with SIMPLE method. More details concerned with the FVM (finite volume method) can be found in Refs. [33, 34].

For these simulations, the calculations were considered converged when the residuals for the mass, momentum and energy between two consecutive iterations were less than 10^{-6}, 10^{-6} and 10^{-8}, respectively. Moreover, under-relaxation factor of 0.7 was imposed for all conservation equations.

4. Description of the Problem

The analyses consider two-dimensional cavities with square cross-section (Fig. 1). Once the developed code is three-dimensional, the two-dimensional simulations performed here are considered with only one element for the Y-direction, where the size that was taken for the depth of the cavity is shown in Table 1. In this same table, the computational and physical parameters used in the present work are presented: Reynolds and Prandtl numbers, cavity domain, independent grid, computational environment and sub-grid constants of Smagorinsky and Prandtl.

Concerning the boundary conditions, the fluid flow in the cavity is generated by the motion of an infinite plate that also represents the upper surface (*XY* plane), where the velocity of the plate is taken as the reference velocity for the computation of the Reynolds number. Additionally, this surface presents the non-slip and the

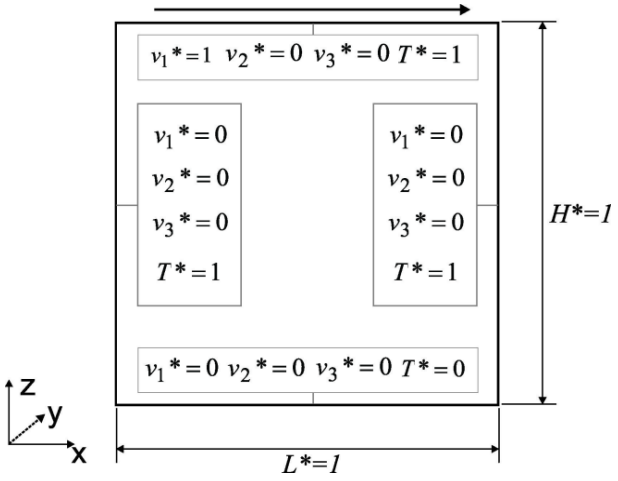

Fig. 1 Cavity flow domain and boundary conditions.

impermeability boundary conditions. In the lateral (*YZ* planes) and lower (*XY* plane) surfaces, the dimensionless velocities are prescribed as null ($V_1^* = V_2^* = V_3^* = 0$). As for the thermal field, the heating of the fluid is a result of imposing a dimensionless temperature of $T^* = 1$ on the upper surface and $T^* = 0$ on the other surfaces. The velocities and temperatures at the cavity corners are assumed the same of the superior and inferior surfaces. It is worthy to reinforce that the quasi-incompressibility approach subdues the spurious oscillations generated at the cavity corners for incompressible flows due to the step changes on the imposition of boundary conditions from lateral surfaces and the corners [29].

The dimensionless terms, represented by the superscript *, are defined as:

$$x_i^* = \frac{x_i}{H} \ (i = 1, 2 \text{ and } 3) \tag{22}$$

$$v_i^* = \frac{v_i}{v_{1\max}} \ (i = 1, 2 \text{ and } 3) \tag{23}$$

$$T^* = \frac{(T - T_{\inf})}{(T_{\sup} - T_{\inf})} \tag{24}$$

where, H is the height of the cavity; v_{1max} is the sliding velocity of the top surface; and T_{sup} and T_{inf} are the largest and the smallest temperatures in the cavity.

The steadiness of the solution is achieved when the relative deviation between two time-averaged temperature profiles at different time steps ("n" and "n + 1") is less than 10^{-6}.

Table 1 Physical and computational parameters that were adopted in the simulations shown in this work.

Parameter	Case 1	Case 2	Case 3
Reynolds number (Re_H)	100	1,000	10,000
Prandtl number (Pr)	1	1	1
Cavity domain (x^*, y^*, z^*)	$1 \times 1 \times 10^{-1} \times 1$	$1 \times 1 \times 10^{-1} \times 1$	$1 \times 1 \times 10^{-2} \times 1$
Independent grid (x^*, y^*, z^*)	$80 \times 1 \times 80$	$80 \times 1 \times 80$	$128 \times 1 \times 128$
Independent grid FLUENT (x^*, y^*, z^*)	$100 \times 1 \times 100$	$120 \times 1 \times 120$	$200 \times 1 \times 200$
Critical time step (s)	4.0×10^{-6}	4.0×10^{-6}	1.0×10^{-6}
Smagorinsky constant (Cs)	0.0	0.23	0.23
Sub-grid Prandtl number (Pr_{sgs})	-	0.6	0.6
Computational environment	Sun Fire X2200, AMD Opteron 1.8 GHz dual core, Infiniband		

5. Results and Discussion

The first step for the evaluation of the numerical method proposed in the present work is the achievement of the appropriate discretization. The grid independence is determined by successive refinements, increasing the number of elements four times from the current mesh size to the next mesh size, until the deviation between time-averaged velocity and temperature profiles was lower than 0.1%. Fig. 2 presents one example of the employment of the grid independence test at Re_H = 100. Fig. 2a presents the time-averaged velocity in Z^* direction (V_3^*) as a function of X^* at Z^* = 0.5, while Fig. 2b shows the time-averaged temperature profile as a function of X^* at Z^* = 0.5. The results are obtained for the following grids: 20 × 20, 40 × 40 and 80 × 80. The results indicate that the grid seems more sensitive for the thermal field than for the velocity field. This behavior was also observed for the other simulations: Re_H = 1,000 and 10,000. In spite of the achievement of a similar behavior for all discretizations employed, the velocity and temperature gradients are smoothed when the grid is coarser.

The next step consists to evaluate qualitatively the temperature fields obtained with the present method for forced convection flows at the steady state for several Reynolds number. To achieve this purpose, a comparison between the topology of the thermal fields obtained with the present method and that one reached with the CFD package FLUENT is performed. Figs. 3a-3c show the topologies of the temperature fields obtained with the present method for the following cases: Re_H = 100; 1,000 and 10,000. Meanwhile, Figs. 3d and 3f show the same temperature topologies for the simulations with FLUENT.

The thermal fields reached with the present method are in very good agreement with those obtained with the commercial CFD package. In spite of this concordance, some differences are observed. For example, the temperature gradients near the upper surfaces seem more intense in the simulations of the present method. Other difference is concerned with the length of the reattachment of the boundary layer in the downstream lower corner, which also seems higher in the present method than in the FLUENT simulations. Moreover, for Re_H = 10,000, the mixture of the temperature field looks more intense for the simulation with the commercial code, mainly in the corner regions.

For the evaluation of the temperature field as a function of the Reynolds number, it is observed that both methods reproduce suitably some characteristics of the flows. For instance, it is observed an asymptotic displacement of the center of the main vortex from the downstream upper region of the cavity toward the center of the cavity as the Reynolds number increases. For the laminar regime, the scalar mixture is dominated by the main vortex (Re_H = 100 and 1,000, Figs. 3a, 3b, 3d and 3e). For two-dimensional turbulent flow (Re_H = 10,000) it is possible to observe the arising of multiple scales and its influence over the energy transport, which becomes to be performed by the

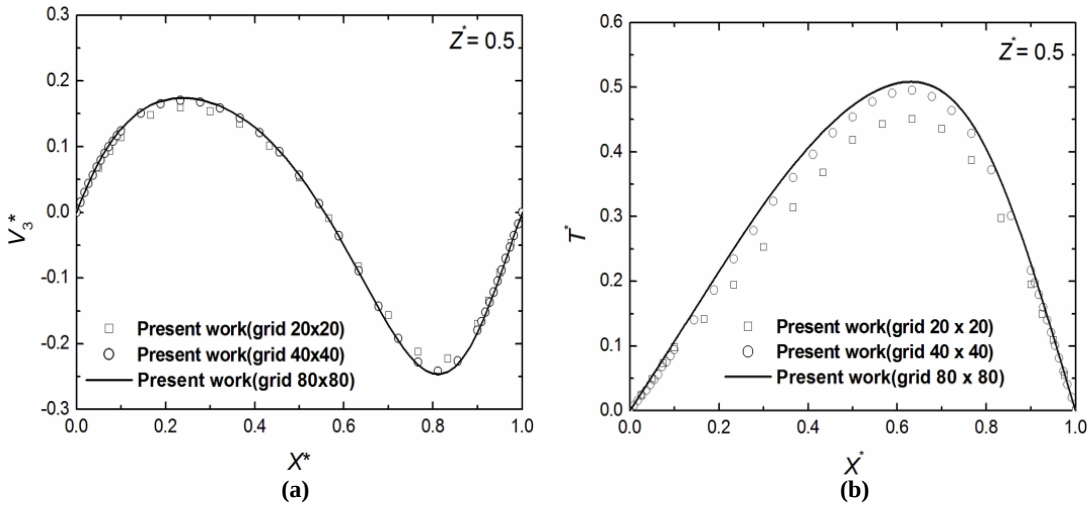

Fig. 2 Grid independence study performed for the flow with Re_H = 100 and Pr = 1.0: (a) time-averaged velocity profile $V_3^* \times X^*$ at Z^* = 0.5; (b) time-averaged temperature profile $T^* \times X^*$ at Z^* = 0.5.

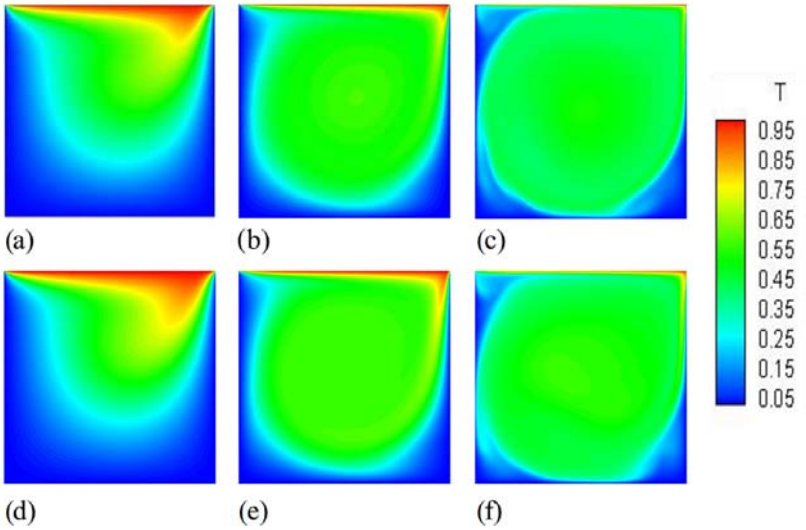

Fig. 3 Topologies of the temperature fields at the steady state for the following cases: Present method—(a) Re_H = 100 and Pr = 1.0; (b) Re_H = 1,000 and Pr = 1.0; (c) Re_H = 10,000 and Pr = 1.0; FLUENT—(d) Re_H = 100 and Pr = 1.0; (e) Re_H = 1,000 and Pr = 1.0; (f) Re_H = 10,000 and Pr = 1.0.

association of the main with secondary vortexes. This observation can be specially performed in the upstream lower and upper corners, Fig. 3c and 3f. This behavior is in agreement with the previous findings of Refs. [9-12].

For the quantitative evaluation of the results obtained with the method used in the present work, the time-averaged velocity and temperature profiles at the cavity center for forced convection flows at Re_H = 100, Re_H = 1,000 and Re_H = 10,000 and Pr = 1 are presented in Figs. 4-9. The profiles obtained here are compared with those ones presented in Refs. [12, 26, 27]. The results are also confronted with the velocity and temperature profiles obtained with FLUENT.

Fig. 4 shows the time-averaged velocity profiles at Re_H = 100 and Pr = 1. Fig. 4a presents the time-averaged velocity profile $V_1^* \times Z^*$ at X^* = 0.5. In general, the temperature profiles are in a very good agreement. Only minor differences are noticed for the profile obtained by Ref. [27] in the region ($0.2 \leq Z^* \leq 0.5$). Fig. 4b depicts the time-averaged velocity profile of $V_3^* \times X^*$ at Z^* = 0.5. It is observed a very good

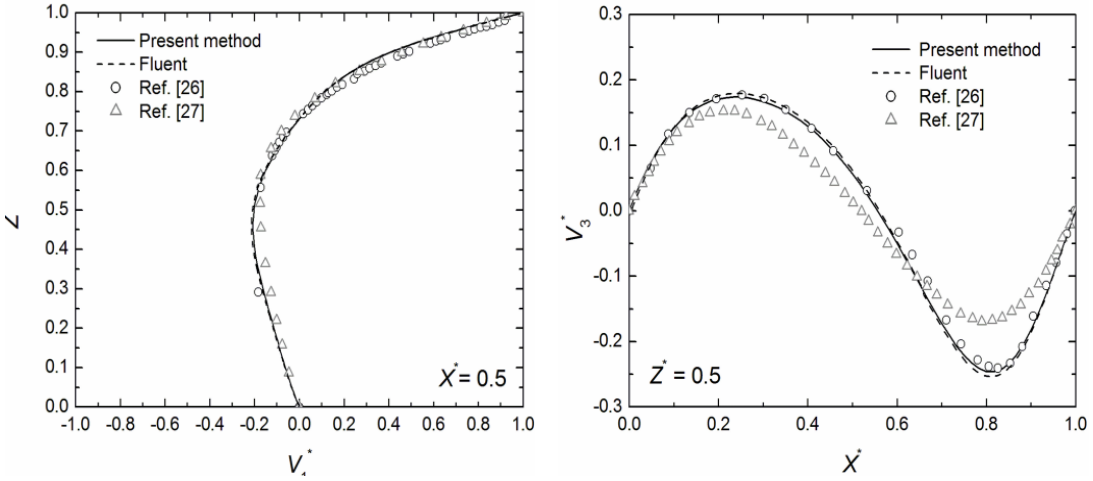

(a) **(b)**

Fig. 4 Time-averaged velocity profiles for a flow with Re_H = 100 and Pr = 1.0 at the steady state: (a) $V_1^* \times Z^*$ at X^* = 0.5; (b) $V_3^* \times X^*$ at Z^* = 0.5.

concordance among the results, with exception for the results of Ref. [27], which reached to differences of approximately 30%. The time-averaged velocity profile obtained in the latter work is smoothed in comparison with the others. This result is similar to that obtained with the present method for a grid of 20 × 20, indicating that the results of Ref. [27] are grid dependent. It is also observed that the insertion of the energy equation in the isothermal method [13] does not modify the velocity field for forced convection flows, which is expected.

Fig. 5 presents the time-averaged temperature profiles at Re_H = 100 and Pr = 1. Fig. 5a shows the time-averaged temperature field $T^* \times Z^*$ at $X^* = 0.5$. All of the results presented a very good agreement. Minor differences are observed for the results of Refs. [26, 27], where the temperature gradients near the upper surface are slightly smoothed in comparison with those predicted in the present work. Fig. 5b illustrates the time-averaged temperature profile $T^* \times X^*$ at $Z^* = 0.5$. In spite of the similarity of all temperature profiles, differences between the results obtained with the present method and FLUENT in comparison with the ones predicted in Refs. [26, 27] are observed. The highest difference is nearly 8% at $X^* = 0.63$. It is also worthy to mention that the simulations of Ref. [12] are isothermal, as a consequence, there is no reliable results for the temperature fields for flows with Re_H > 100. Other purpose of this work is to obtain a theoretical recommendation for the time-averaged temperature fields, allowing the evaluation of new developed methods.

Fig. 6 presents the time-averaged velocity at Re_H = 1,000 and Pr = 1. Figs. 6a and 6b exhibit the time-averaged profiles $V_1^* \times Z^*$ at $X^* = 0.5$ and $V_3^* \times X^*$ at $Z^* = 0.5$, respectively. For both profiles, the results obtained with the present method and FLUENT are in close agreement with those predicted in Ref. [12], which is the benchmark solution. Only slight differences are obtained for the velocity gradients near the surfaces. On the opposite, a comparison with the other results of Refs. [26, 27] shows a poor agreement. It is observed only a similar trend among the results. The numerical results obtained here corroborate the previous observation of Ref. [12], which states that the results of Ref. [26] are grid dependent for $Re_H \geq 1{,}000$. This same remark can be extrapolated for the results of Ref. [27].

Fig. 7 presents the time-averaged temperature profiles at Re_H = 1,000 and Pr = 1. Fig. 7a shows the time-averaged temperature field $T^* \times Z^*$ at $X^* = 0.5$. The profiles reached with the present method and with the CFD package are in very good agreement. The temperature profile obtained with FLUENT is approximately 4% higher than that found with the present

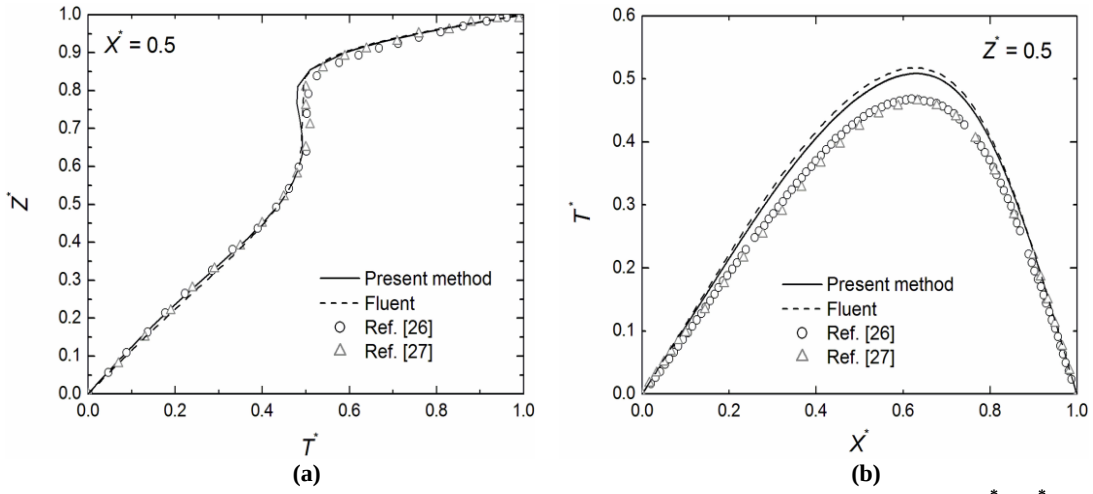

(a) (b)

Fig. 5 Time-averaged temperature profiles for a flow with Re_H = 100 and Pr = 1.0 at the steady state: (a) $T^* \times Z^*$ at X^* = 0.5; (b) $T^* \times X^*$ at Z^* = 0.5.

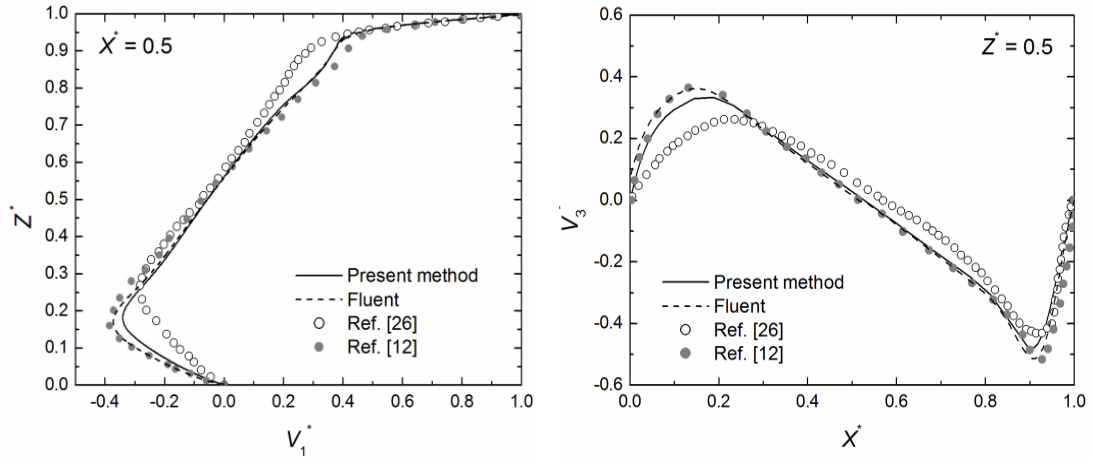

(a) (b)

Fig. 6 Time-averaged velocity profiles for a flow with Re_H = 1,000 and Pr = 1.0 at the steady state: (a) $V_1^* \times Z^*$ at X^* = 0.5; (b) $V_3^* \times X^*$ at Z^* = 0.5.

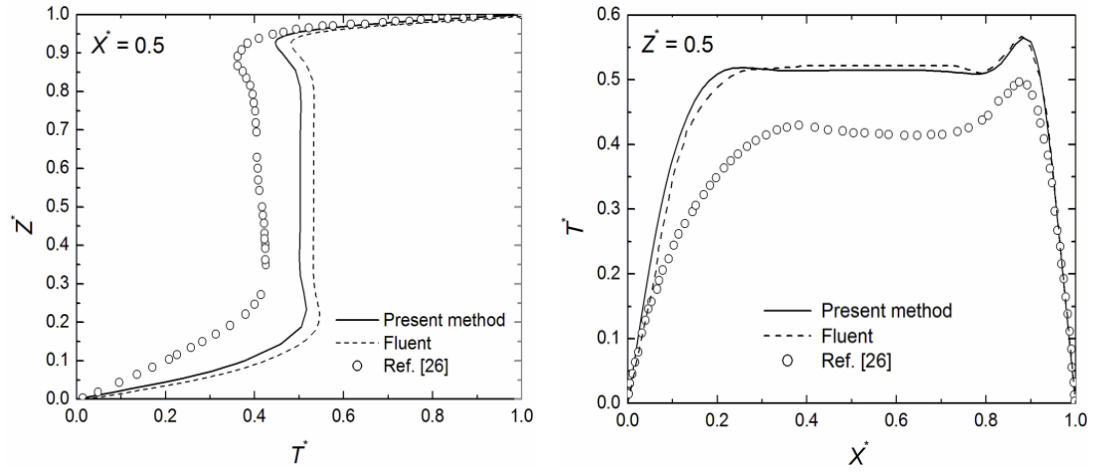

(a) (b)

Fig. 7 Time-averaged temperature profiles for a flow with Re_H = 1,000 and Pr = 1.0 at the steady state: (a) $T^* \times Z^*$ at X^* = 0.5; (b) $T^* \times X^*$ at Z^* = 0.5.

method. Fig. 7b illustrates the time-averaged temperature profile $T^* \times X^*$ at $Z^* = 0.5$. Minor deviations are found for the temperature profiles for the region ($0.18 \le X^* \le 0.28$). The profile obtained with the present method is nearly 5% hotter than that predicted with FLUENT. As observed for the velocity fields, the results obtained by Ref. [26] are grid dependent, showing only a trend of the behavior obtained with the numerical methodologies used in the present work. A noteworthy fact is that the results obtained for a grid with 20 × 20 elements in the present method are in good agreement with those predicted in Ref. [26]. The results of Ref. [27] have large discrepancies, and will not be presented.

For the two-dimensional turbulent flow (Re_H = 10,000 and Pr = 1.0), the time-averaged velocity and temperature fields are presented in Figs. 8 and 9, respectively. Fig. 8a shows the time-averaged velocity profile $V_1^* \times Z^*$ at $X^* = 0.5$ and Fig. 8b shows the time-averaged velocity profile $V_3^* \times X^*$ at $Z^* = 0.5$. The results obtained with the present method, FLUENT and Ref. [12] presented an excellent agreement. Minor deviations are observed for the velocity numerical simulations performed here and those of Ref. [12]. The highest difference is lower than 2%. For the time-averaged temperature field, Fig. 7a shows the profile $T^* \times Z^*$ at $X^* = 0.5$ and Fig. 7b depicts the profile $T^* \times X^*$ at $Z^* = 0.5$. Once the results of Ref. [26] are in total disagreement with the other results for the velocity and temperature fields, these results will not be shown for the temperature field with the purpose to avoid confusion. These discrepancies can be associated with many factors. For example, the use of dependent grids, low order of discretization for the solution by means of DNS and the inexistence of any closure model for the treatment of turbulence into the RANS or LES framework. The numerical results obtained with the present method and those reached with FLUENT are in very good agreement. In average, the temperature profiles obtained with FLUENT are hotter than that obtained with the present method. The highest deviations happen for the profile $T^* \times X^*$ for the region of $0.63 \le X^* \le 0.94$, where differences of almost 5% are noticed. Other important aspect is the increase of the velocity and temperature gradients with the increase of Reynolds number. Moreover, the quantitative results corroborated what was observed for the temperature topologies, i.e., the center of the main vortex displaces from the downstream upper region of the cavity toward the center of the cavity and the multiplicity of scales increases as the Reynolds number increases. This is in agreement with the previous observations of Refs. [8-12].

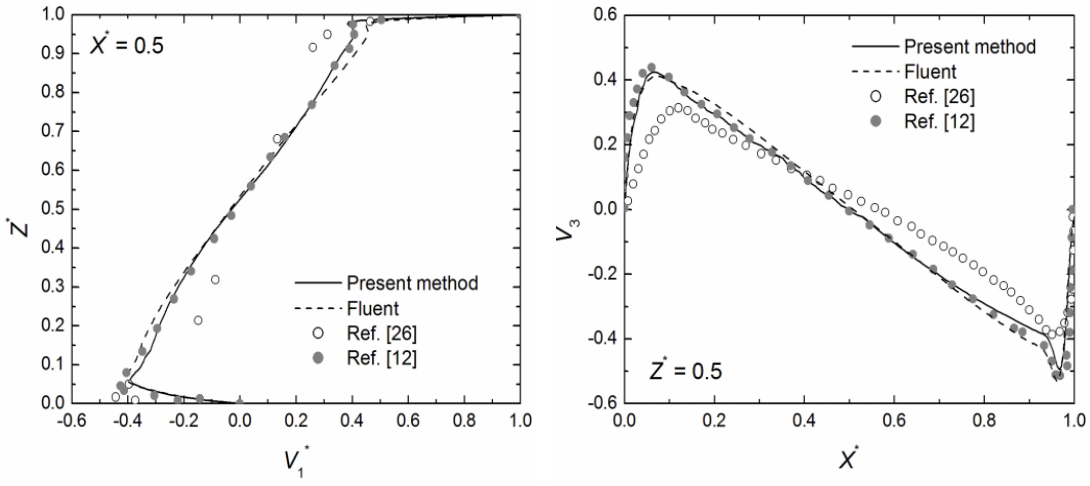

(a) (b)

Fig. 8 Time-averaged velocity profiles for a flow with Re_H = 10,000 and Pr = 1.0 at the steady state: (a) $V_1^* \times Z^*$ at $X^* = 0.5$; (b) $V_3^* \times X^*$ at $Z^* = 0.5$.

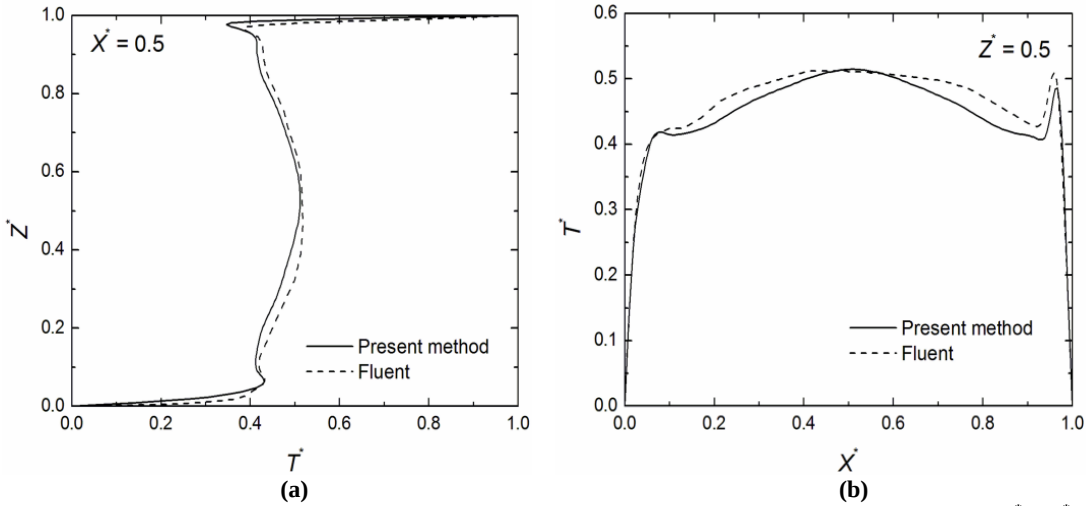

Fig. 9 Time-averaged temperature profiles for a flow with Re_H = 10,000 and Pr = 1.0 at the steady state: (a) $T^* \times Z^*$ at X^* = 0.5; (b) $T^* \times X^*$ at Z^* = 0.5.

6. Conclusions

This work presented a numerical study of lid-driven cavity flows with forced convection heat transfer in both laminar and two-dimensional turbulent regimes for a flow at the steady state. The main purpose here was the development of a numerical method for the suitable prediction of non-isothermal, incompressible, laminar and turbulent flows. The numerical solutions for the present method were obtained with the finite element method and a second-order temporal iterative explicit scheme of Taylor-Galerkin. The turbulence was treated with the large eddy simulation with the sub-grid model of Smagorinsky. Topologies, as well as, time-average velocity and temperature profiles were obtained using the new developed method to simulate forced convection lid-driven cavity flows for various Reynolds numbers (Re_H = 100, 1,000 and 10,000) and for a fixed Prandtl number (Pr = 1.0). All evaluations were performed when the flow reaches the steady state.

This work presented a numerical study of lid-driven cavity flows with forced convection heat transfer in both laminar and two-dimensional turbulent regimes for a flow at the steady state. The main purpose here was the development of a numerical method for the suitable prediction of non-isothermal, incompressible, laminar and turbulent flows. The numerical solutions for the present method were obtained with the finite element method and a second-order temporal iterative explicit scheme of Taylor-Galerkin. The turbulence was treated with the large eddy simulation with the sub-grid model of Smagorinsky. Topologies, as well as, time-average velocity and temperature profiles were obtained using the new developed method to simulate forced convection lid-driven cavity flows for various Reynolds numbers (Re_H = 100, 1,000 and 10,000) and for a fixed Prandtl number (Pr = 1.0). All evaluations were performed when the flow reaches the steady state.

Acknowledgments

E.D. dos Santos thanks CAPES, Brasília, DF, Brasil, by his doctorate scholarship; L.A.O. Rocha and F.H.R. França thanks CNPq, Brasília, DF, Brasil, for research grant. The authors also thank the National Center of Supercomputation (CESUP-RS) for the technical support.

References

[1] H. Tennekes, J.L. Lumley, A First Course in Turbulence, MIT Press, USA, 1972.

[2] S.B. Pope, Turbulent Flows, Cambridge University Press, New York, USA, 2008.

[3] M. Lesieur, O. Métais, P. Comte, Large-Eddy Simulations of Turbulence, Cambridge University Press, New York, 2005.

[4] L. Wang, Y. Dong, X. Lu, An investigation of turbulent open channel flow with heat transfer by large eddy

simulation, Comput. Fluids 34 (2005) 23-47.

[5] D.C. Wilcox, Turbulence Modeling for CFD, 2nd ed., DCW Industries, Canada, 2002.

[6] P. Saugat, Large Eddy Simulation for Incompressible Flows: An Introduction, 3rd ed., Springer Berlin Heidelberg, Berlin, 2006.

[7] A.K. Prasad, J.R. Koseff, Combined forced and natural convection heat transfer in a deep lid-driven cavity flow, Int. J. Heat Fluid Flow 17 (1996) 460-467.

[8] E.D. dos Santos, G.L. Piccoli, F.H.R. França, A.P. Petry, Analysis of mixed convection in transiente laminar and turbulent flows in driven cavities, Int. J. Heat Mass Transf. 54 (2011) 4585-4595.

[9] W. Kim, S. Menon, An unsteady incompressible Navier-Stokes solver for large eddy simulation of turbulent flows, Int. J. Numer. Meth. Fluids 31 (1999) 983-1017.

[10] Y. Zang, R.L. Street, J.R. Koseff, A dynamic mixed sub-grid scale model and its application to turbulent recirculating flows, Phys. Fluids A 5 (1993) 3186-3196.

[11] E. Erturk, C. Gökçöl, Fourth-order compact formulation of Navier-Stokes equations and driven cavity flow at high Reynolds number, Int. J. Numer. Meth. Fluids 50 (2006) 421-436.

[12] U. Guia, K.N. Ghia, C.T. Shin, High-Re solutions for incompressible flow using the Navier-Stokes equations and multigrid method, J. Comput. Phys. 48 (1982) 387-411.

[13] A.P. Petry, A.M. Awruch, Large eddy simulation of three-dimensional turbulent flows by finite element method, J. of the Braz. Soc. of Mech. Sci. & Eng. 28 (2006) 224-232.

[14] K.J. Hsieh, F.S. Lien, Numerical modeling of buoyancy-driven turbulent flows in enclosures, Int. J. Heat Fluid Flow 25 (2004) 659-670.

[15] S.H. Peng, L. Davidson, Large eddy simulation for turbulent buoyant flow in a confined cavity, Int. J. Heat Fluid Flow 22 (2001) 323-331.

[16] L. Valencia, J. Pallares, I. Cuesta, F.X. Grau, Turbulent Rayleigh-Bénard convection of water in cubical cavities: A numerical and experimental study, Int. J. Heat Mass Transf. 50 (2007) 3203-3215.

[17] L. Agrawal, J.C. Mandal, A.G. Marathe, Computations of laminar and turbulent mixed convection in a driven cavity using pseudo-compressibility approach, Comput. Fluids 30 (2001) 607-620.

[18] S.K. Lee, C.K. Chen, Finite element solutions of laminar and turbulent mixed convection in a driven cavity, Int. J. Num. Meth. Fluids 23 (1996) 47-64.

[19] D. Bouris, G. Bergeles, Two-dimensional LES of vortex shedding from a square cylinder, J. Wind. Eng. Ind. Aerod. 80 (1999) 31-46.

[20] A. Horvat, I. Kljenak, J. Marn, Two-dimensional large-eddy simulation of turbulent natural convection due to internal heat generation, Int. J. Heat Mass Transf. 44 (2001) 3985-3995.

[21] E.D. dos Santos, Analysis of non-isothermal, incompressible flows, using large eddy simulations and finite element method, Master Thesis, Federal University of Rio Grande do Sul, Porto Alegre, 2007. (in Portuguese)

[22] J.N. Reddy, D.K. Gartling, The Finite Element Method in Heat Transfer and Fluid Dynamics, CRC, Florida, 1994.

[23] J. Donea, A Taylor-Galerkin method for convective transport problems, Int. J. Numer. Methods Eng. 20 (1984) 101-119.

[24] M. Kawahara, H. Hirano, A finite element method for high Reynolds number viscous fluid flow using two step explicit scheme, Int. J. Numer. Meth. Fluids 3 (1983) 137-163.

[25] J. Smagorinsky, General circulation experiment with the primitive equations, I. The basic experiment, Mon. Weath. 91 (1963) 99-164.

[26] M. Nallasamy, K.K. Prasad, On cavity flow at high Reynolds numbers, J. Fluid Mech. 79 (1977) 391-414.

[27] C.F. Lange, Simulation of non-isothermal, incompressible flows using finite element method with penalty function, Master Thesis, Federal University of Rio Grande do Sul, Porto Alegre, 2007. (in Portuguese)

[28] Fluent (Version 6.3.16), ANSYS, Inc., 2007.

[29] P.M. Gresho, R.L. Sani, Incompressible Flow and the Finite Element Method, Advection-Diffusion and Isothermal Laminar Flow, John Wiley & Sons Ltd., UK, 1999.

[30] P.H. Gaskell, A.K.C. Lau, Curvative-compensated convective transport: SMART, a new boundedness-preserving transport algorithm, Int. J. Numer. Meth. Fluids 8 (6) (1988) 617-641.

[31] B.P. Leonard, The ultimate conservative difference scheme applied to unsteady one-dimensional advection, Comput. Methods Appl. Mech. Engrg. 88 (1991) 17-74.

[32] J. Zhu, W. Rodi, A low dispersion and bounded convection scheme, Comput. Methods Appl. Mech. Energy 92 (1991) 225-232.

[33] S.V. Patankar, Numerical Heat Transfer and Fluid Flow, McGraw Hill, New York, 1980.

[34] H.K. Versteeg, W. Malalasekera, An Introduction to Computational Fluid Dynamics: The Finite Volume Method, Longman, England, 1995.